

EGG-WM--9039

DE91 006106

SCALING CONSIDERATIONS FOR MODELING THE IN SITU VITRIFICATION PROCESS

M. A. Langerman

R. J. MacKinnon

Published September, 1990


EG&G Idaho, Inc.
Idaho Falls, ID 83415

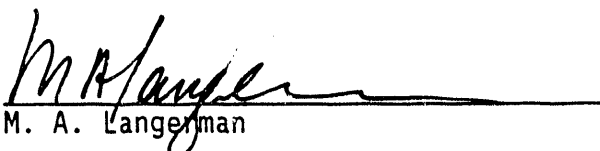
Prepared for the
U. S. Department of Energy
Idaho Operations Office
Under DOE Contract No. DE-AC07-76ID01570

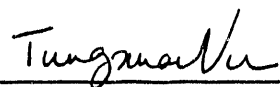
MASTER

DISTRIBUTION OF THIS DOCUMENT IS UNLIMITED

SCALING CONSIDERATIONS FOR MODELING
THE IN SITU VITRIFICATION PROCESS
EGG-WM-9039

Approved By:  Date: 9/18/90
S. K. Merrill, Manager
In Situ Vitrification

Prepared By:  Date: 9/14/90
M. A. Langerman

Reviewed By:  Date: 9/14/90
Vu X. Tung
Technical Reviewer

ABSTRACT

Scaling relationships for modeling the in situ vitrification waste remediation process are documented based upon similarity considerations derived from fundamental principles. Requirements for maintaining temperature and electric potential field similarity between the model and the prototype are determined as well as requirements for maintaining similarity in off-gas generation rates. A scaling rationale for designing reduced-scale experiments is presented and the results are assessed numerically.

NOMENCLATURE

<u>Symbol</u>	<u>Description of Symbol</u>
σ	electrical conductivity
V	voltage
j	current density
Ω	domain descriptor
Γ	boundary descriptor
f	proportionality constant
L	characteristic length
T	material temperature
C_m	mixture volumetric heat capacity
c	charge
k	mixture thermal conductivity
q'''	volumetric joule heat
U	liquid velocity
h	heat transfer coefficient
θ	temperature difference
H	latent heat of fusion
s'	melt front velocity
ρ	gas density
t	time
ϵ	soil porosity
κ	soil permeability
p	gas pressure
μ	gas viscosity
k	mixture thermal conductivity
Q	volumetric gas production rate
V_0	superficial velocity
β	gas compressibility
γ	coefficient of thermal expansion
g	gravitational constant
Q	volumetric off-gas release rate
P	power

TABLE OF CONTENTS

ABSTRACT.....	ii
NOMENCLATURE.....	iii
TABLE OF CONTENTS.....	iv
1.0 INTRODUCTION	1
2.0 SIMILARITY REQUIREMENTS	2
2.1 Potential Field.....	2
2.2 Temperature Field	5
2.3 Off-Gas Generation.....	9
3.0 SCALING RATIONALE.....	12
4.0 NUMERICAL ASSESSMENT.....	17
5.0 CONCLUSIONS	24
6.0 REFERENCES	25

FIGURES

Figure 2.1 Idealized ISV configuration	3
Figure 3.1 Finite element model of the ISV process; a) top view, b) isometric view	18
Figure 3.2 Temperature at $x/x_{max}=0.33$ and $z/z_{max}=0.30$ (linear and quadratic power scaling).....	20
Figure 3.3 Temperature at $x/x_{max}=0.40$ and $z/z_{max}=0.70$ (linear and quadratic power scaling).....	21
Figure 3.4 Joule heat at $x/x_{max}=0.33$ and $z/z_{max}=0.30$ (linear and quadratic power scaling).....	22
Figure 3.5 Temperature at $x/x_{max}=0.33$ and $z/z_{max}=0.30$ (distorted heat transfer coefficient).....	23

1.0 INTRODUCTION

The in situ vitrification (ISV) process is being proposed as a means of remediating hazardous wastes buried at the Idaho National Engineering Laboratory (INEL).^{1,2} Prior to implementation, however, the program has been directed to assess the safety of the process and to determine the suitability of the process to the local conditions existing at the INEL. In response, the ISV program has proposed a strategy to address the issues of safety and suitability that includes an integral package composed of analytical analyses and experimental tests to simulate the general ISV process.

The analysis package which has been proposed, and is currently under development, simulates the ISV process with a set of mathematical equations derived from fundamental physical and chemical principles. The testing program currently being considered will simulate the ISV process with scaled experiments. The two projects will be integrally related, the analysis package playing a key role in planning upcoming experiments and interpreting data while the testing program provides data for assessing the accuracy and completeness of the analytical results. The success of this strategy, however, is conditional upon the acquisition of relevant data whether analytically or experimentally. Consequently, implicit within the ISV program objectives is the requirement to develop a rationale for scaling between the prototype process and the scaled experiments. Stated otherwise, to assure the applicability of the analytical and experimental data obtained, the model ISV process must maintain dynamic similarity with the prototype ISV process. Requirements for maintaining dynamic similarity between the model and the prototype are the subject of this report.

Three important areas for scaling the ISV process are addressed and include: 1) the temperature field, 2) the potential field, and 3) the off-gas generation rates. Areas not addressed here include: 1) the flow and combustion of off-gases, 2) the melt natural circulation, and 3) the soil/waste characterization. Section 2 of this report presents the similarity considerations derived from first principles. Section 3 presents the scaling rationale developed from the similarity considerations of Section 2. Section 4 presents a numerical assessment of the scaling rationale using a finite element numerical model of the ISV process.³ Section 5 presents conclusions reached from this investigation and Section 6 lists the cited references.

2.0 SIMILARITY REQUIREMENTS

The concept of similarity is derived from geometry: two bodies are considered similar when their corresponding linear dimensions are in constant ratio to one another. The concept of dynamic similarity demands in addition that all the other physical quantities involved in a given pair of systems, such as forces, time intervals, velocities, and temperatures, are respectively proportional to one another. In this section, the requirements for maintaining dynamic similarity in scaled ISV experiments are documented. These requirements are based upon the fundamental physics governing the respective potential and temperature fields and the off-gas generation rates.

A two-dimensional cross-sectional view of an idealized ISV configuration is shown in Figure 2.1. The problem domain is partitioned into four regions; the electrodes Ω_e , the liquid melt Ω_l , the surrounding solid soil Ω_s , and the atmosphere Ω_a . Boundaries are indicated by $\Gamma_{i,j}$, where i and j denote adjacent zones. The moving boundaries are Γ_{ls} and Γ_{la} . Outward unit normal vectors for the liquid melt and electrodes are n_l and n_e , respectively.

2.1 Potential Field

The potential field is governed by the charge conservation equation⁴ given here in vector form

$$\nabla \cdot \sigma \nabla V = 0 \quad \text{in } \Omega_e \cup \Omega_l \cup \Omega_s \quad (2.1)$$

and the boundary conditions

$$V = \hat{V} \quad \text{on } \Gamma_{ss} \quad (2.2)$$

$$-\sigma \nabla V \cdot n = j_n \quad \text{on } \Gamma_{ea} \quad (2.3)$$

$$-\sigma \nabla V \cdot n = 0 \quad \text{on } \Gamma_{sa} \cup \Gamma_{la} \quad (2.4)$$

where V is voltage and σ is electrical conductivity which is represented as a scalar function of T , the temperature. In boundary condition (2.2) the voltage is specified at points along boundary Γ_{ss} . In boundary conditions (2.3) and (2.4) the normal outward component of the current density, j , is specified along boundaries Γ_{ea} , Γ_{sa} and Γ_{la} , where j is defined as:

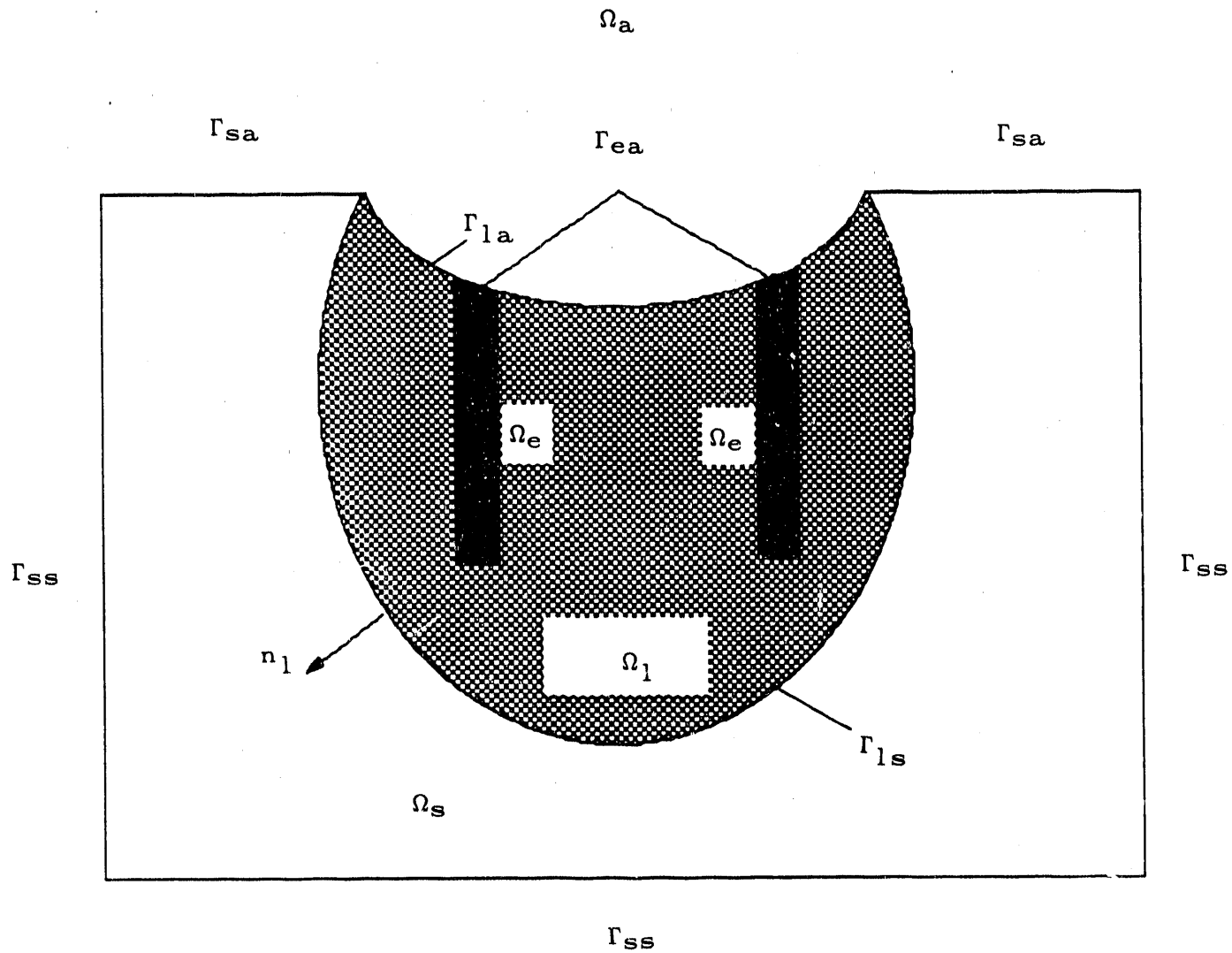


Figure 2.1 Idealized ISV configuration.

$$\mathbf{j} = -\sigma \nabla V. \quad (2.5)$$

The governing equation, (2.1), expanded in cartesian coordinates is

$$\frac{\partial}{\partial x_1} \left(\sigma_1 \frac{\partial V_1}{\partial x_1} \right) + \frac{\partial}{\partial y_1} \left(\sigma_1 \frac{\partial V_1}{\partial y_1} \right) + \frac{\partial}{\partial z_1} \left(\sigma_1 \frac{\partial V_1}{\partial z_1} \right) = 0 \quad (2.6)$$

where subscript 1 indicates the prototype with a similar equation for the model (subscript 2), similarly, the boundary conditions are:

$$V_1 = \hat{V}_1 \quad (2.7)$$

$$-\sigma \frac{\partial V_1}{\partial n_1} = j_n, \quad (2.8)$$

$$-\sigma \frac{\partial V_1}{\partial n_1} = 0. \quad (2.9)$$

It is now assumed that the two systems are physically similar, i.e., corresponding quantities in 1 and 2 are in constant ratio to each other. (The conditions necessary to render this assumption valid are the derived dimensionless groups presented later.) Therefore, for all lengths, including coordinates x, y, z of a point, the appropriate proportionality factor is defined by:

$$f_l = \frac{L_2}{L_1}. \quad (2.10)$$

The remaining factors are:

$$\text{(voltage)} \rightarrow f_v = \frac{V_2}{V_1}, \quad (2.11)$$

$$\text{(electrical conductivity)} \rightarrow f_\sigma = \frac{\sigma_2}{\sigma_1}, \quad (2.12)$$

and

$$\text{(current density)} \rightarrow f_j = \frac{j_2}{j_1}. \quad (2.13)$$

Substituting (2.10)-(2.13) into governing equation (2.6) and boundary conditions (2.7)-(2.9), for system 2, results in

$$\frac{f_{\sigma}f_v}{f_1^2} \left[\frac{\partial}{\partial x_1} (\sigma_1 \frac{\partial V_1}{\partial x_1}) + \frac{\partial}{\partial y_1} (\sigma_1 \frac{\partial V_1}{\partial y_1}) + \frac{\partial}{\partial z_1} (\sigma_1 \frac{\partial V_1}{\partial z_1}) \right] = 0 \quad (2.14)$$

and

$$f_{\sigma} V_1 = f_{\sigma} \hat{V}_1 \quad (2.15)$$

$$-\frac{f_{\sigma}f_v}{f_1} \sigma_1 \left(\frac{\partial V_1}{\partial n_1} \right) = f_j j_{n1} \quad (2.16)$$

$$-\frac{f_{\sigma}f_v}{f_1} \sigma_1 \left(\frac{\partial V_1}{\partial n_1} \right) = 0. \quad (2.17)$$

Note that the governing equation places no requirement on the proportionality factors since $f_{\sigma}f_v/f_1^2$ can be divided out and is, therefore, arbitrary [similarly with the insulated boundary condition (2.17)]. Regarding boundary condition (2.16), system 2 is identical to system 1 if

$$\frac{f_{\sigma}f_v}{f_1} = f_j, \quad (2.18)$$

or equivalently,

$$\frac{j_2 L_2}{\sigma_2 V_2} = \frac{j_1 L_1}{\sigma_1 V_1}. \quad (2.19)$$

Therefore, similarity considerations regarding the potential field require that

$$\frac{jL}{\sigma V} = \text{constant}. \quad (2.20)$$

The following section presents the similarity requirements resulting from the energy equation.

2.2 Temperature Field

The temperature field is governed by the energy equation given below in vector form as

$$C_m(\mathbf{U} \cdot \nabla T) = \nabla \cdot \mathbf{k} \nabla T + q''' \quad \text{in } \Omega_e \cup \Omega_1 \cup \Omega_s. \quad (2.21)$$

with the boundary conditions

$$T = T_0 \quad \text{on } \Gamma_{ss} \quad (2.22)$$

$$-\mathbf{k} \nabla T \cdot \mathbf{n} = h_n \theta \quad \text{on } \Gamma_{sa} \cup \Gamma_{la} \cup \Gamma_{ea} \quad (2.23)$$

$$k_1 \nabla T \cdot \mathbf{n} - k_s \nabla T \cdot \mathbf{n} = \rho_s H \mathbf{s}' \cdot \mathbf{n} \quad \text{on } \Gamma_{ls} \quad (2.24)$$

$$T = T_m \quad \text{on } \Gamma_{ls} \quad (2.25)$$

where T is the temperature, T_m is the melt temperature, C_m is the mixture volumetric heat capacity, k is the mixture thermal conductivity, $q''' = j^2 / \sigma = \sigma |\nabla V|^2$ is the joule heat source, $U = [u, v, w]$ is the liquid melt velocity (equal to zero in Ω_s), h_n is the heat transfer coefficient from soil to air ($\theta = T - T_a$), H is the latent heat of fusion, and s' is the velocity of the moving boundary, Γ_{ls} .

Remark 1: Although the steady-state energy equation is used [equation (2.21)], dimensionless groups arising from the transient terms are accounted for in the melt front velocity boundary condition.

Following the same procedure as before, the respective proportionality factors are:

$$\text{(velocity)} \rightarrow f_u = \frac{u_2}{u_1}, \quad (2.26)$$

$$\text{(density)} \rightarrow f_\rho = \frac{\rho_2}{\rho_1}, \quad (2.27)$$

$$\text{(thermal conductivity)} \rightarrow f_k = \frac{k_2}{k_1}, \quad (2.28)$$

$$\text{(specific heat)} \rightarrow f_C = \frac{C_2}{C_1}, \quad (2.29)$$

$$\text{(temperature)} \rightarrow f_T = \frac{T_2}{T_1}, \quad (2.30)$$

$$\text{(heat of fusion)} \rightarrow f_H = \frac{H_2}{H_1}, \quad (2.31)$$

and

$$\text{(melt front velocity)} \rightarrow f_s = \frac{s'_2}{s'_1}. \quad (2.32)$$

Substituting (2.26)-(2.32) into governing equation (2.21), for the model, results in

$$\begin{aligned} & \frac{f_u f_T}{f_1} \left(u_1 \frac{\partial T_1}{\partial x_1} + v_1 \frac{\partial T_1}{\partial y_1} + w_1 \frac{\partial T_1}{\partial z_1} \right) = \\ & \frac{f_k f_T}{f_C f_1^2} \left[\frac{\partial}{\partial x_1} \left(k_1 \frac{\partial T_1}{\partial x_1} \right) + \frac{\partial}{\partial y_1} \left(k_1 \frac{\partial T_1}{\partial y_1} \right) + \frac{\partial}{\partial z_1} \left(k_1 \frac{\partial T_1}{\partial z_1} \right) \right] + \\ & \frac{f_\sigma f_v^2}{f_C f_1^2} \left[\sigma_1 |\nabla V_1|^2 \right]. \end{aligned} \quad (2.33)$$

Boundary conditions (2.22)-(2.25) reduce to

$$-\frac{f_k f_T}{f_l} k_1 \left(\frac{\partial T_1}{\partial n_1} \right) = f_h f_T h_1 \theta_1, \quad (2.34)$$

and

$$\left[\frac{f_k f_T}{f_l} k_1 \left(\frac{\partial T_1}{\partial n_1} \right) \right]_l - \left[\frac{f_k f_T}{f_l} k_1 \left(\frac{\partial T_1}{\partial n_1} \right) \right]_s = f_H f_s f_\rho H \rho_s s'. \quad (2.35)$$

The above results yield the following requirements:

$$\frac{f_u f_T}{f_l} = \frac{f_k f_T}{f_C f_l^2} = \frac{f_\sigma f_v^2}{f_C f_l^2}, \quad (2.36)$$

$$\frac{f_k f_T}{f_l} = f_h f_T, \quad (2.37)$$

and

$$\frac{f_k f_T}{f_l} = f_H f_s f_\rho. \quad (2.38)$$

Therefore,

$$\frac{C_1 u_1 L_1}{k_1} = \frac{C_2 u_2 L_2}{k_2}, \quad (2.39)$$

$$\frac{k_1 T_1}{\sigma_1 V_1^2} = \frac{k_2 T_2}{\sigma_2 V_2^2}, \quad (2.40)$$

$$\frac{C_1 u_1 T_1 L_1}{\sigma_1 V_1^2} = \frac{C_2 u_2 T_2 L_2}{\sigma_2 V_2^2}, \quad (2.41)$$

$$\frac{h_1 L_1}{k_1} = \frac{h_2 L_2}{k_2}, \quad (2.42)$$

and

$$\frac{k_1 T_1}{\rho_1 L_1 H_1 s'_1} = \frac{k_2 T_2}{\rho_2 L_2 H_2 s'_2}. \quad (2.43)$$

Note that (2.41) is simply a combination of (2.39) and (2.40). Similarity considerations regarding the temperature fields, therefore, require the following:

$$\frac{CuL}{k}(\text{Reynolds number} \times \text{Prandtl number} = \text{Peclet number}) = \text{constant}, \quad (2.44)$$

$$\frac{hL}{k}(\text{Nusselt number}) = \text{constant}, \quad (2.45)$$

$$\frac{kT}{\sigma V^2} = \text{constant}, \quad (2.46)$$

and

$$\frac{kT}{\rho L H s'} = \text{constant}. \quad (2.47)$$

Recall that the temperature field and the potential field are coupled through the generation term, $\sigma|\nabla V|^2$, and the dependence of σ on T . So considering these two field variables together (i.e., T and V), a different approach from that above can be taken as follows. From equations (2.1)-(2.47), there results 10 variables common to each system, namely $L, k, \rho, u, T, \sigma, V, h, j$ and s' . The units of each are

$$L = \text{m},$$

$$k = \text{J/s m K},$$

$$\rho = \text{kg/m}^3,$$

$$u = \text{m/s},$$

$$T = \text{K},$$

$$\sigma = \text{c}^2/\text{m}^2 \text{ s N},$$

$$V = \text{Nm/c},$$

$$h = \text{J/s m}^2 \text{ K},$$

$$j = \text{c/s m}^2,$$

and

$$s' = \text{m/s},$$

or 5 basic units (i.e., mass or force, length, time, temperature or energy, and charge). From the Buckingham Pi theorem⁵ these 10 variables can be replaced by 5 independent dimensionless groups, namely (2.20) of the previous section and (2.44)-(2.47) above.

The following section presents the similarity requirements regarding the off-gas release rates.

2.3 Off-Gas Generation

For flow through a porous medium the equations of continuity and motion may be replaced by:^{6,7}

$$\epsilon \frac{\partial \rho}{\partial t} = -(\nabla \cdot \rho \mathbf{V}_O) + Q \quad \text{in } \Omega_S \quad (2.48)$$

and

$$\mathbf{V}_O = -\frac{\kappa}{\mu}(\nabla p - \rho \mathbf{g}), \quad \text{in } \Omega_S \quad (2.49)$$

where ϵ is the soil porosity, κ is the soil permeability, p is the gas pressure, μ is the gas viscosity, ρ is the gas density, Q is the mass production rate of gas per unit volume, and \mathbf{V}_O is the superficial velocity (volume rate of flow through a unit cross-sectional area of porous medium).

Combining the above two equations, neglecting gravity, and assuming an ideal gas results in

$$\rho \epsilon \left(\beta \frac{\partial p}{\partial t} - \gamma \frac{\partial T}{\partial t} \right) = \nabla \cdot \frac{\rho \kappa}{\mu} \nabla p + Q \quad \text{in } \Omega_S \quad (2.50)$$

where $\beta=1/p$ is the gas compressibility and $\gamma=1/T$ is the coefficient of thermal expansion. The boundary and initial conditions are

$$p = \hat{p} = 0 \quad \text{on } \Gamma_{SS} \cup \Gamma_{Sa} \quad (2.51)$$

$$\hat{V}_O = -\frac{\kappa}{\mu}(\nabla p - \rho \mathbf{g}) \cdot \mathbf{n} \quad \text{on } \Gamma_{ls} \quad (2.52)$$

and

$$p = p_O(\text{initial}) = 0 \quad \text{in } \Omega_S. \quad (2.53)$$

Remark 2: Boundary condition (2.50) represents the inflow of gas \hat{V}_O across melt boundary Γ_{ls} into the liquid melt. Note that (2.50) is simply (2.47) defined along and normal to Γ_{ls} .

Proceeding as before

$$\begin{aligned} & \frac{f_\rho f_\epsilon}{f_t} (\rho_1 \epsilon_1) (f_\beta f_p \beta_1 \frac{\partial p_1}{\partial t_1} - f_\gamma f_T \gamma_1 \frac{\partial T_1}{\partial t_1}) = \\ & \frac{f_\rho f_\kappa f_p}{f_\mu f_1^2} \left\{ \frac{\partial}{\partial x_1} \left(\frac{\rho_1 \kappa_1}{\mu_1} \right) \frac{\partial p_1}{\partial x_1} + \frac{\partial}{\partial y_1} \left(\frac{\rho_1 \kappa_1}{\mu_1} \right) \frac{\partial p_1}{\partial y_1} + \right. \\ & \quad \left. \frac{\partial}{\partial z_1} \left(\frac{\rho_1 \kappa_1}{\mu_1} \right) \frac{\partial p_1}{\partial z_1} \right\} + f_Q Q_1 \quad \text{in } \Omega_s, \end{aligned} \quad (2.54)$$

with

$$f_p p_1 = f_p \hat{p}_1 = 0 \quad \text{on } \Gamma_{ss} \cup \Gamma_{sa}, \quad (2.55)$$

and

$$f_p p_1 = f_p p_{01} = 0 \quad \text{in } \Omega_s. \quad (2.56)$$

Equations (2.54)-(2.56) yield the following result

$$\frac{f_\epsilon f_\rho f_\beta f_p}{f_t} = \frac{f_\epsilon f_\rho f_\gamma f_T}{f_t} = \frac{f_\rho f_\kappa f_p}{f_\mu f_1^2} = f_Q. \quad (2.57)$$

Therefore,

$$\frac{\beta_1 p_1}{\gamma_1 T_1} = \frac{\beta_2 p_2}{\gamma_2 T_2}, \quad (2.58)$$

$$\frac{\epsilon_1 \beta_1 \mu_1 L_1^2}{\kappa_1 t_1} = \frac{\epsilon_2 \beta_2 \mu_2 L_2^2}{\kappa_2 t_2}, \quad (2.59)$$

$$\frac{\epsilon_1 \gamma_1 T_1 \mu_1 L_1^2}{\kappa_1 t_1 p_1} = \frac{\epsilon_2 \gamma_2 T_2 \mu_2 L_2^2}{\kappa_2 t_2 p_2}, \quad (2.60)$$

$$\frac{\epsilon_1 \rho_1 \beta_1 p_1}{Q_1 t_1} = \frac{\epsilon_2 \rho_2 \beta_2 p_2}{Q_2 t_2}, \quad (2.61)$$

$$\frac{\epsilon_1 \rho_1 \gamma_1 T_1}{Q_1 t_1} = \frac{\epsilon_2 \rho_2 \gamma_2 T_2}{Q_2 t_2}, \quad (2.62)$$

and

$$\frac{\rho_1 \kappa_1 p_1}{\mu_1 L_1^2 Q_1} = \frac{\rho_2 \kappa_2 p_2}{\mu_2 L_2^2 Q_2}. \quad (2.63)$$

The first relationship, (2.58) is trivial since for an ideal gas $\beta=1/p$ and $\gamma=1/T$. Closer examination further indicates that (2.59) is a restatement of (2.60). Similarly (2.61) is a restatement of (2.62) and a combination of (2.62) and (2.63) results in (2.59). Therefore, similarity requirements relating to off-gas generation rates result in two independent dimensionless groups which must remain constant between the model and prototype. These groups are

$$\frac{\epsilon \beta \mu L^2}{\kappa t} = \text{constant}, \quad (2.64)$$

and

$$\frac{\epsilon \rho \gamma T}{Q t} = \text{constant}. \quad (2.65)$$

Before proceeding, it should be noted that the first dimensionless group above is actually a combination of two groups obtained from analyzing the modified continuity and motion equation separately. In doing so the following two groups result:

$$\frac{\epsilon L}{V_0 t} = \text{constant} \quad (2.66)$$

and

$$\frac{V_0 \mu L}{\kappa p} = \text{constant}. \quad (2.67)$$

Using an approach similar to that discussed for the potential and temperature fields, it can be shown that, for off-gas release, 5 variables are common between the model and prototype with a total of 3 basic units [or 6 variables if equation (2.64) is replaced with equations (2.66) and (2.67)]. From the Buckingham Pi theorem, therefore, the problem reduces from 5 variables to 2 independent dimensionless groups, namely (2.64) and (2.65) above [(or in the alternate case the problem reduces from 6 variables to 3 independent dimensionless groups, namely (2.65)-(2.67)].

The following section develops a scaling rationale from the similarity relationships discussed above and presents some observations regarding the various dimensionless groups.

3.0 SCALING RATIONALE

This section develops a rationale for scaling between the prototype ISV process and scaled experiments. The rationale is based upon the similarity requirements developed in the previous section and summarized below

$$\frac{jL}{\sigma V} = \text{constant}, \quad (3.1)$$

$$\frac{\rho CuL}{k} = \text{constant}, \quad (3.2)$$

$$\frac{hL}{k} = \text{constant}, \quad (3.3)$$

$$\frac{kT}{\sigma V^2} = \text{constant}, \quad (3.4)$$

$$\frac{kT}{\rho L H s'} = \text{constant}, \quad (3.5)$$

$$\frac{\epsilon \beta \mu L^2}{\kappa t} = \text{constant}, \quad (3.6)$$

and

$$\frac{\epsilon \rho \gamma T}{Q t} = \text{constant}. \quad (3.7)$$

As noted previously, (3.6) can be replaced with

$$\frac{\epsilon L}{V_0 t} = \text{constant} \quad (3.8)$$

and

$$\frac{\gamma_0 \mu L}{\kappa p} = \text{constant}, \quad (3.9)$$

by including the superficial velocity, V_0 .

A scaling rationale can now be developed from these dimensionless groups. First (3.1) and (3.3)-(3.5) are rearranged as follows:

$$\frac{j_2}{j_1} = \frac{\sigma_2 L_1 V_2}{\sigma_1 L_2 V_1}, \quad (3.10)$$

$$\frac{L_2}{L_1} = \frac{h_1 k_2}{h_2 k_1}, \quad (3.11)$$

$$\frac{V_2}{V_1} = \sqrt{\frac{\sigma_1 k_2 T_2}{\sigma_2 k_1 T_1}}, \quad (3.12)$$

and

$$\frac{s_2'}{s_1'} = \left(\frac{\rho_1 L_1 H_1}{\rho_2 L_2 H_2} \right) \left(\frac{k_2 T_2}{k_1 T_1} \right). \quad (3.13)$$

Several preliminary observations can be made from (3.10)-(3.13) above. First, looking at the power requirements, P, where P is defined as

$$P = q'''(\text{volume}) = \frac{j^2}{\sigma} L^3. \quad (3.14)$$

Multiplying and dividing both sides of (3.10) by jL^3/σ for system 2 and 1, respectively, results in

$$\frac{P_2}{P_1} = \frac{j_2 L_2^2 V_2}{j_1 L_1^2 V_1}.$$

Substituting (3.10) in for j_2/j_1

$$\frac{P_2}{P_1} = \frac{\sigma_2 V_2^2 L_2}{\sigma_1 V_1^2 L_1}$$

and combining with (3.12) results in

$$\frac{P_2}{P_1} = \frac{k_2 T_2 L_2}{k_1 T_1 L_1}. \quad (3.15)$$

Now, if it is assumed that kT is the same in the model and prototype (which will shortly be shown to hold if the material in the model and prototype are the same and physical similarity is maintained), then the powers have to be in linear ratio to some characteristic length of each system, such as the electrode separation. If it is further assumed that the material density and latent heat of fusion are the same in each system then from (3.13)

$$\frac{s_2'}{s_1'} = \frac{L_1}{L_2}. \quad (3.16)$$

Equation (3.16) indicates that similarity precludes equal melt front velocities. This conclusion can be reached alternatively by first assuming equal melt front velocities in each system, then from (3.13) and (3.15)

$$\frac{P_2}{P_1} = \frac{\rho_2 L_2^2 H_2}{\rho_1 L_1^2 H_1}$$

and again assuming equal material properties, then

$$\frac{P_2}{P_1} = \frac{L_2^2}{L_1^2},$$

a result which is inconsistent with (3.15) and the assumption of the equal material properties. Consequently, to maintain similarity between the model and the prototype requires that the melt front velocity be higher and the time scale be reduced in the model.

In (3.10)-(3.13), there are 8 unknowns (assuming all of the prototype variables are fixed) but only 4 equations thus indicating no unique scaling rationale exists. However, if it is assumed that the material temperature at each corresponding location in the model and prototype is the same, then a unique scaling rationale results as follows.

If the material temperature in the model and prototype is the same at corresponding locations then the material properties must also be equal at these points since the properties are functions of temperature. Therefore, from (3.10)-(3.13),

$$\frac{L_2}{L_1} = \frac{h_1}{h_2},$$

$$\frac{V_2}{V_1} = 1,$$

$$\frac{j_2}{j_1} = \frac{L_1}{L_2},$$

and

$$\frac{s_2'}{s_1'} = \frac{L_1}{L_2}.$$

So, for example, if it is desired to model at a physical scale of $\frac{1}{2}$ then

$$h_2 = 2h_1,$$

$$V_2 = V_1,$$

$$j_2 = 2j_1,$$

and the melt front velocity would be 2 times the melt front velocity of the prototype, that is

$$s'_2 = 2s'_1.$$

Next, (3.6) and (3.7) are rearranged as

$$\frac{\epsilon_2 \mu_2 L_2^2}{\epsilon_1 \mu_1 L_1^2} = \frac{\kappa_2 p_2 t_2}{\kappa_1 p_1 t_1}, \quad (3.17)$$

and

$$\frac{Q_2}{Q_1} = \frac{\epsilon_2 \rho_2 t_1}{\epsilon_1 \rho_1 t_2}, \quad (3.18)$$

where, from (3.16),

$$\frac{t_1}{t_2} = \frac{L_1 s'_2}{L_2 s'_1} = \frac{L_1^2}{L_2^2}. \quad (3.19)$$

From (3.17)-(3.19) and the constraint of identical materials

$$p_2 = p_1$$

and

$$\frac{Q_2}{Q_1} = \frac{L_1^2}{L_2^2}.$$

Again if a physical scale of $\frac{1}{2}$ is selected, then the following results:

$$Q_2 = 4Q_1,$$

and from (3.8)

$$V_{o_2} = V_{o_1} \left(\frac{L_2}{L_1} \frac{t_1}{t_2} \right) = 2V_{o_1}.$$

Finally, the ratio of the volume rate of off-gas release, Q , for this example can be calculated as

$$\frac{Q_2}{Q_1} = \frac{V_{o_2}(\text{area})_2}{V_{o_1}(\text{area})_1} = \frac{V_{o_2} L_2^2}{V_{o_1} L_1^2} = 2 \left(\frac{1}{4} \right) = \frac{1}{2}.$$

The following section presents a numerical assessment of the scaling relationships discussed above.

4.0 NUMERICAL ASSESSMENT

This section presents results from a numerical assessment of the scaling rationale discussed in the preceding section. The numerical model is the same as that used in the investigation documented in reference 3. The numerical approach is an application of the finite element method to a method of weighted residuals statement of the governing equations and boundary conditions.

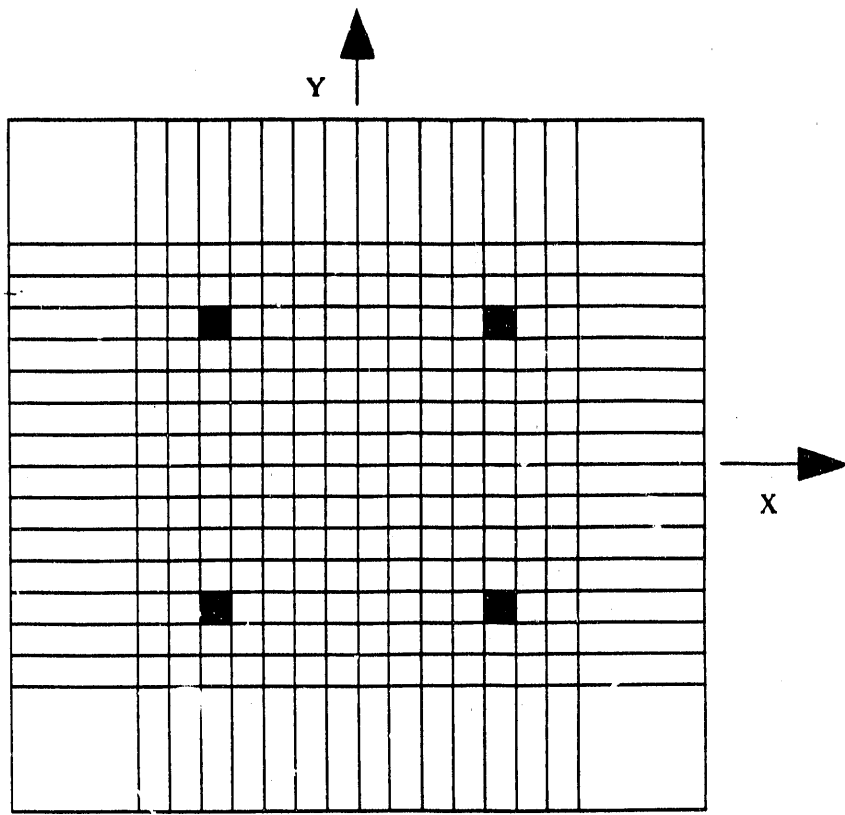
Figure 3.1 shows the finite element discretization used to perform the calculations. The electrode placement is indicated by shading. Four calculations were performed. First, a base case calculation was performed to simulate the prototype ISV process. Second, a one-half scaled model calculation was conducted under the constraints of maintaining similarity which included increasing the surface heat transfer coefficient by a factor of 2. Third, a calculation was performed to assess the distortion resulting from scaling powers quadratically to maintain the same melt front velocities in the model and the prototype. Finally, since manipulation of the surface heat transfer coefficient would be difficult during the management an experiment, a fourth calculation was conducted to assess the importance of this similarity requirement.

It should be noted that steady-state numerical calculations were performed. Assessment of the scaling effects during a transient is beyond the scope of this investigation. Nevertheless, the steady-state model affords a means of addressing the fundamental scaling principles derived in the preceding section.

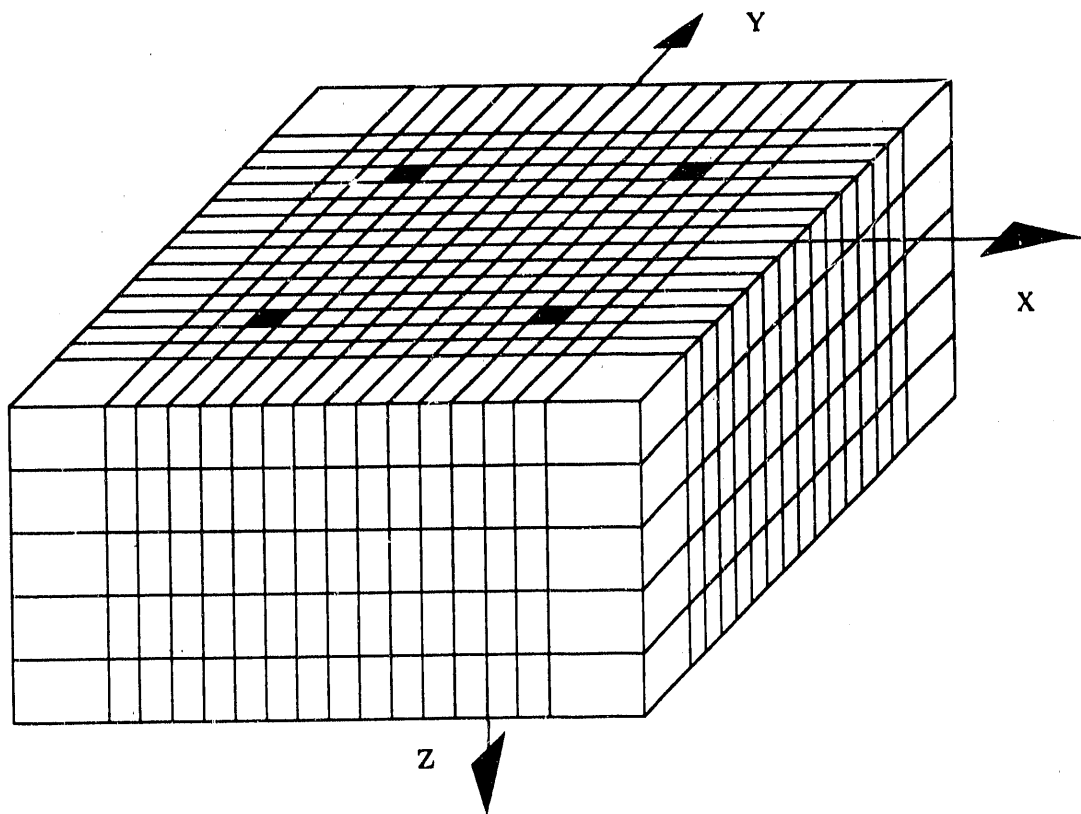
For convenience, the proposed scaling rationale is assessed in terms of the calculated temperature fields and the calculated joule heat distributions. The results presented are for points lying on a line parallel to the y axis and at selected values of x and z (elevation). The results are presented in terms of the proportionality factors (f's) defined for each variable in section 2 and written generally as

$$f_{\xi} = \frac{\xi_{\text{model}}}{\xi_{\text{prototype}}},$$

where ξ is the variable of interest (i.e., temperature, joule heat, etc).



(a)



(b)

Figure 3.1 Finite element model of the ISV process; a) top view, b) isometric view.

Figures 3.2 and 3.3 compare the calculated temperature fields (in terms of f_T) for the cases of quadratic and linear power scaling. The results shown are for two elevations and for two relative values of x (see Figure 3.1). For an ideal model, the value of f_T would be unity. As indicated, the temperature field for the case of quadratic power scaling is significantly distorted both on the lateral plane and in the axial direction. On the other hand, the calculated temperature field for the linear power scaling case approaches that of the ideal field with slight discrepancies indicated in Figure 3.3 near the domain boundary; the inherent result of numerical approximation.

Figure 3.4 compares the calculated joule heat fields ($f_{q'''}$) for the two power scaling cases. For linear power scaling, $f_{q'''}$ is essentially constant at a value near the ideal value of 4. Again the quadratic scaling case produces a distorted source field, however, the distortion appears to be relatively constant except at the boundaries where the source field approaches zero. The ratio of the joule heat between the linear and quadratic scaling cases is approximately 2 which is the expected value based upon the scaling relationships developed in the previous section. The relatively low heat source terms which occur in the case of quadratic power scaling would produce a melt front velocity equal to that of the prototype (based upon scaling relationships), however, they would also produce a temperature field significantly distorted and lower in magnitude than that of the prototype (Figures 3.2 and 3.3). Since these distortions vary as the ratio of the model-to-prototype length scales squared, they would become significantly more pronounced as the model scale is reduced.

Figure 3.5 compares the temperature field for the case when the heat transfer coefficient is ideally maintained at a value twice that of the prototype with the case when the heat transfer coefficient is essentially equal to that of the prototype. These results were obtained assuming a uniform soil medium with the soil material properties obtained from reference 8. The analysis further assumed that convective effects are negligible and the heat loss at the surface is radiation dominated.⁹ The comparison shown in Figure 3.5 indicates that the largest difference in f_T occurs near the boundary of the domain and the distortion in the case of the latter calculation is less than 1%. Based upon steady-state calculations and a model scale of one-half, it appears that the heat transfer coefficient similarity constraint may be relaxed without introducing a significant distortion in the model. This similarity constraint, however, may be less flexible as the scale is reduced.

The following section presents conclusions reached from this investigation.

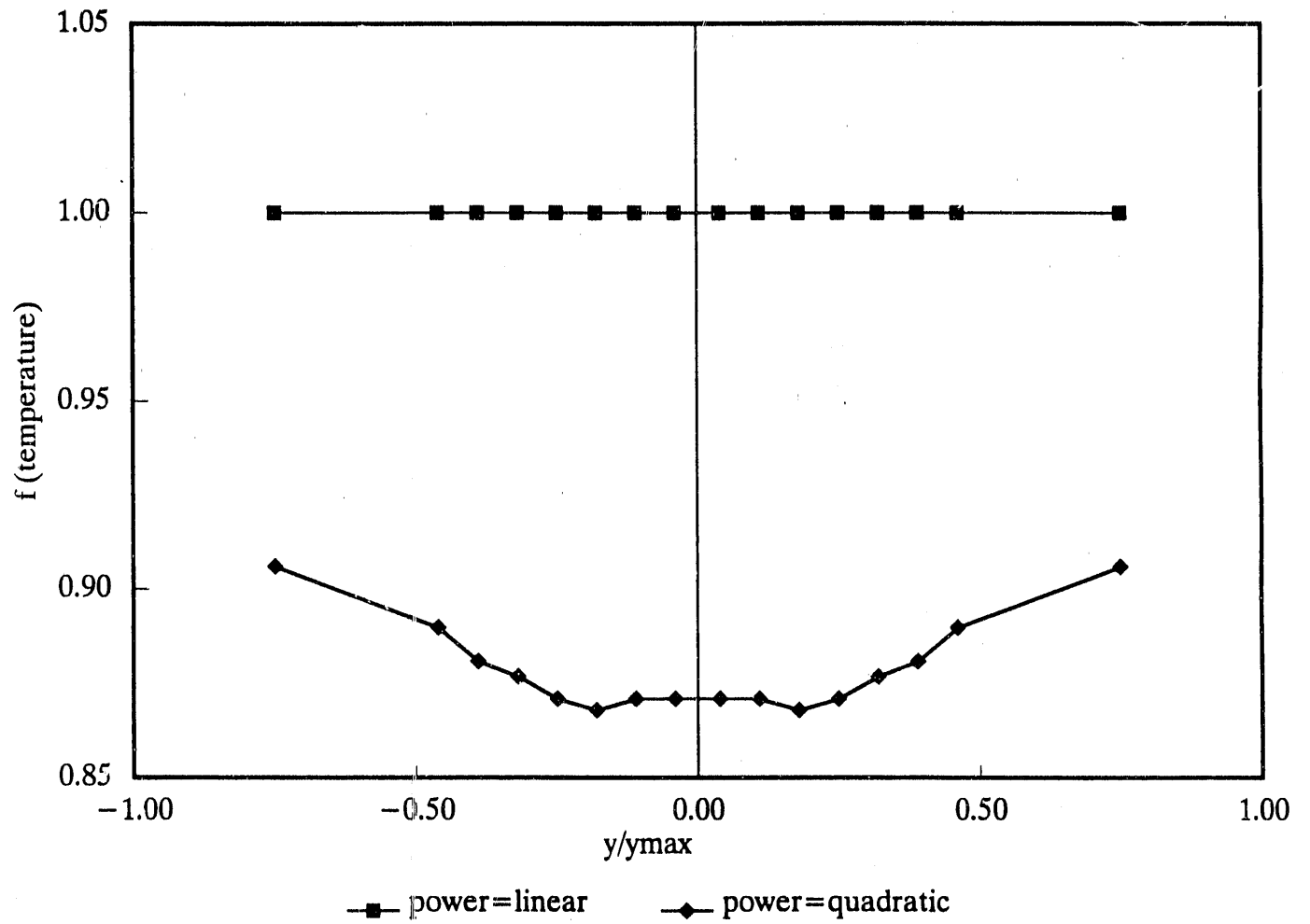


Figure 3.2 Temperature at $x/x_{max}=0.33$ and $z/z_{max}=0.30$ (linear and quadratic power scaling).

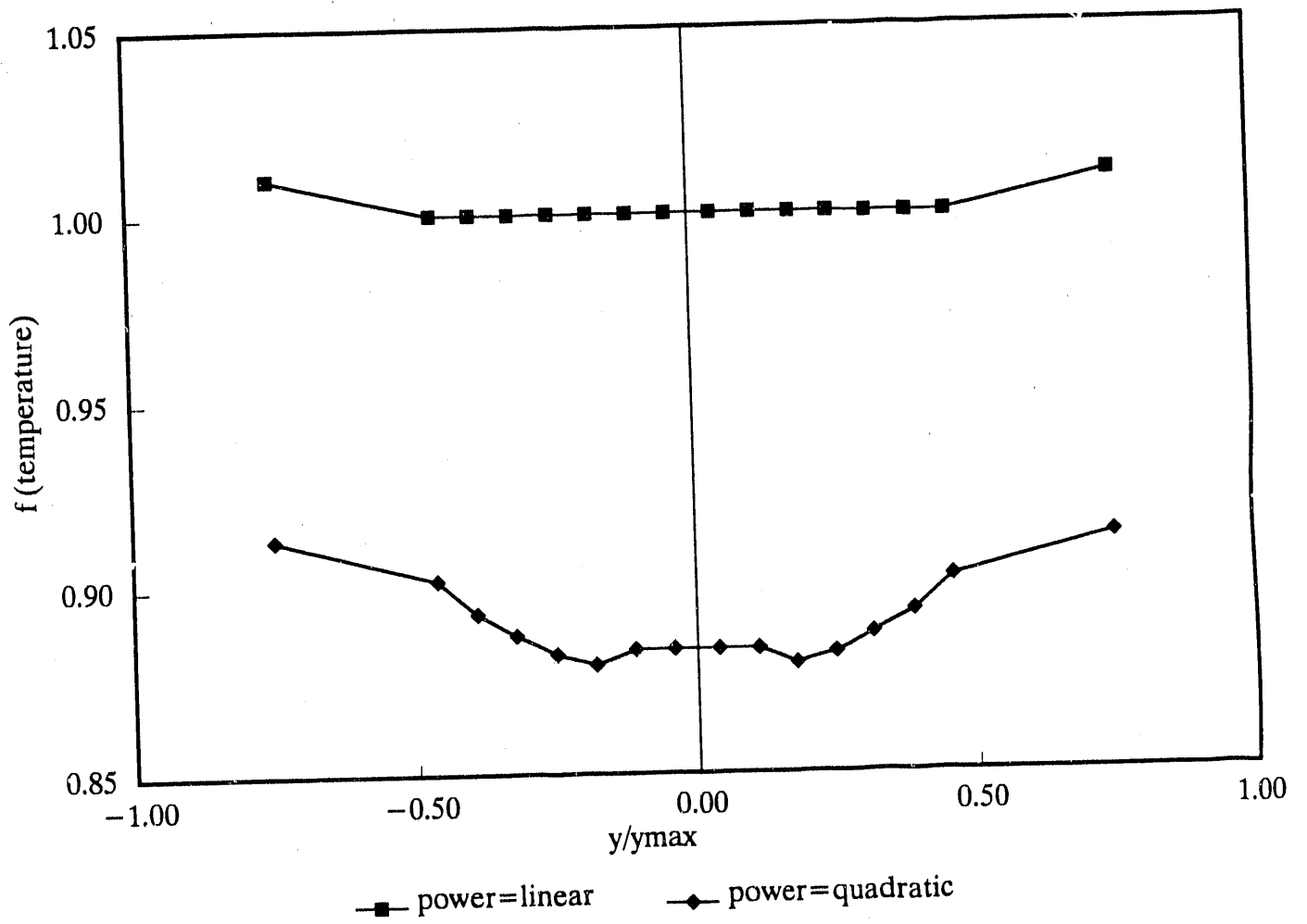


Figure 3.3 Temperature at $x/x_{max}=0.40$ and $z/z_{max}=0.70$ (linear and quadratic power scaling).

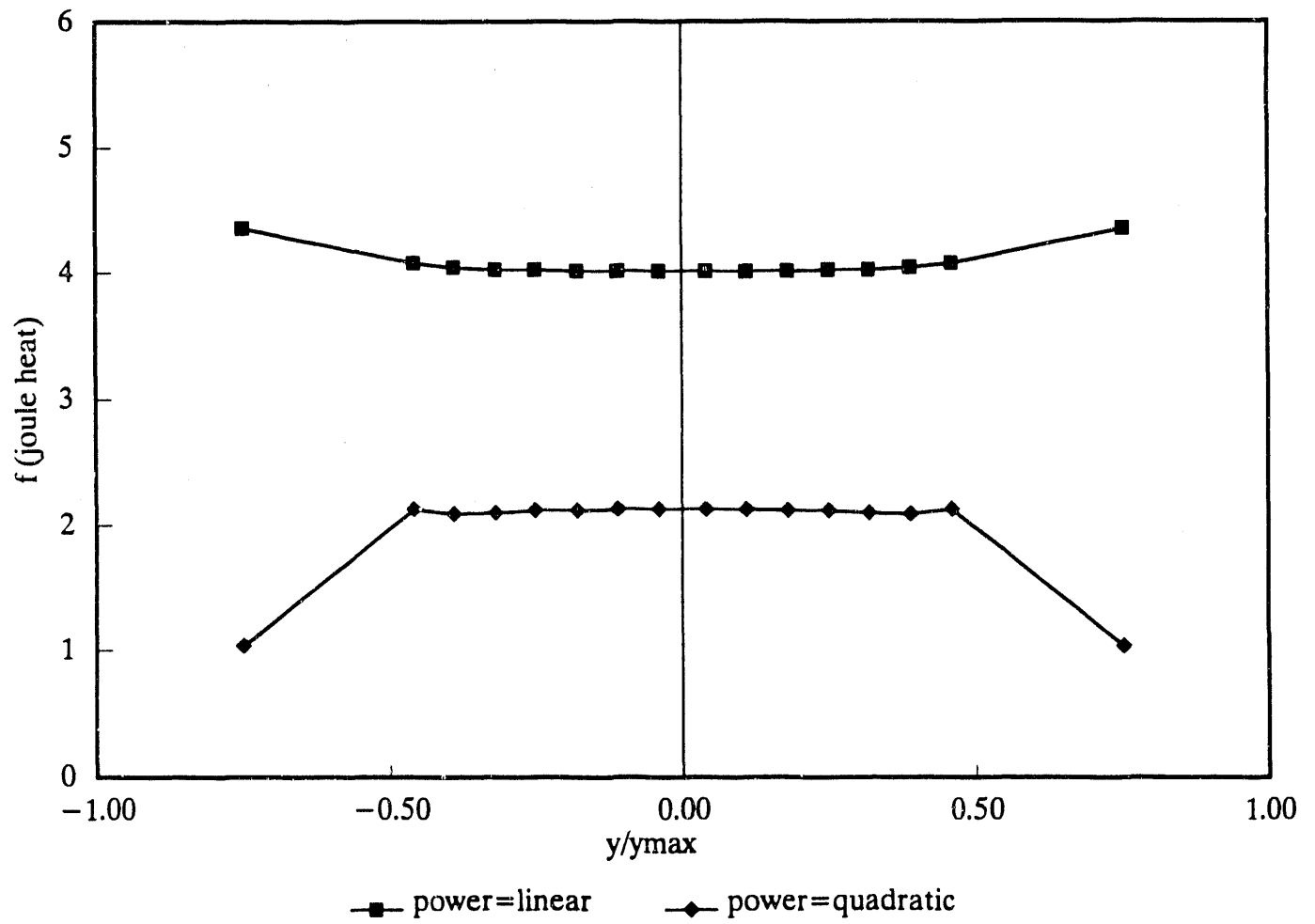


Figure 3.4 Joule heat at $x/x_{max}=0.33$ and $z/z_{max}=0.30$ (linear and quadratic power scaling).

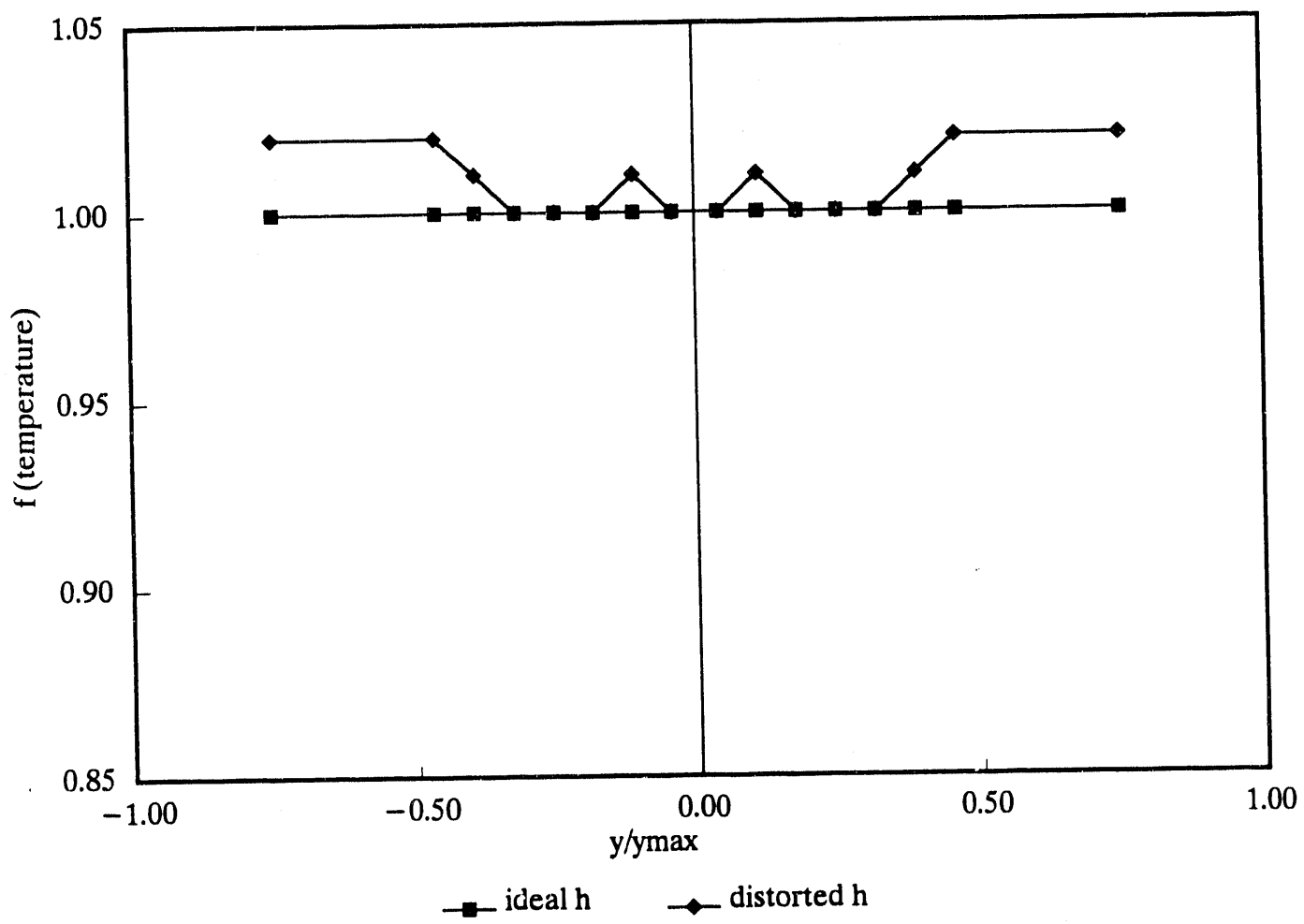


Figure 3.5 Temperature at $x/x_{max}=0.33$ and $z/z_{max}=0.30$ (distorted heat transfer coefficient).

5.0 CONCLUSIONS

Consideration of temperature and potential field phenomena and off-gas generation rates results in seven dimensionless parameters which must remain constant between model and prototype to produce dynamic similarity between ISV processes. These dimensionless groups dictate a scaling rationale from which it is concluded that the appropriate power scaling approach is to scale power by the ratio of characteristic lengths between the model and the prototype. Ideally, the surface heat transfer coefficient should be inversely proportional to this length ratio, however, steady-state calculations indicate that this scaling requirement may be relaxed without introducing significant scaling distortions in the model.

It should be noted that the conclusions reached above regarding power scaling and heat transfer coefficient requirements are based, in part, upon steady-state calculations. It is recommended that, as an extension to this investigation, calculations be performed to investigate transient scaling effects on the model ISV process.

6.0 REFERENCES

1. Arrenholtz, D.A., et.al., "In Situ Vitrification Program Treatability Investigation Workplan," Draft, EGG-WM-9072, June 1990.
2. MacKinnon, R.J., et.al., "In Situ Vitrification Model Development and Implementation Plan," Revision 1.0, EGG-WM-9036, August 1990.
3. Langerman, M.A., "Steady-State Modeling Considerations and Calculated Results For the ISV Process: A 3-D Finite Element Analysis of Coupled Thermal-Electric Fields", EGG-WM-9052, September 1990.
4. Corson, D.R. and P. Lorrain, Introduction to Electromagnetic Fields and Waves, W.H. Freeman and Company, San Francisco and London, 1962.
5. Buckingham, E., "Model Experiments and the Forms of Empirical Equations", Trans. ASME, 37 (1915), 263.
6. Bird, R.B., et.al, Transport Phenomena, John Wiley & Sons, Inc, November, 1966.
7. Brinkman, H.C., Appl. Sci. Research, A1, 27-34, 81-86 (1947).
8. Buelt, et.al., "In-situ Vitrification of Transuranic Wastes: An Updated Systems Evaluation and Applications Assessment, PNL-4800 Suppl.1 UC-70, Pacific Northwest Laboratory, March 1987.
9. P.E. Murray, et.al., "A Preliminary Numerical Study of Heat Transport During In Situ Vitrification of Soil," EGG-WM-9038, June 1990.

END

DATE FILMED

02 / 26 / 91

